Jay T. Pukrushpan
e-mail: pukrushp@umich.edu

Huei Peng[*]

Anna G. Stefanopoulou

Automotive Research Center,
Department of Mechanical Engineering,
University of Michigan,
Ann Arbor, Michigan 48109-2125

Control-Oriented Modeling and Analysis for Automotive Fuel Cell Systems

Fuel Cells are electrochemical devices that convert the chemical energy of a gaseous fuel directly into electricity. They are widely regarded as a potential future stationary and mobile power source. The response of a fuel cell system depends on the air and hydrogen feed, flow and pressure regulation, and heat and water management. In this paper, we develop a dynamic model suitable for the control study of fuel cell systems. The transient phenomena captured in the model include the flow and inertia dynamics of the compressor, the manifold filling dynamics (both anode and cathode), reactant partial pressures, and membrane humidity. It is important to note, however, that the fuel cell stack temperature is treated as a parameter rather than a state variable of this model because of its long time constant. Limitations and several possible applications of this model are presented. [DOI: 10.1115/1.1648308]

1 Introduction

Fuel cell stack systems are under intensive development for mobile and stationary power applications. In particular, Proton Exchange Membrane (PEM) Fuel Cells (also known as Polymer Electrolyte Membrane Fuel Cells) are currently in a relatively more mature stage for ground vehicle applications. Recent announcements of GM "AUTOnomy" concept and federal program "FreedomCAR" are examples of major interest from both the government and automobile manufacturers regarding this alternative energy conversion concept.

To compete with existing internal combustion engines, fuel cell systems must operate at similar levels of performance. Transient behavior is one of the key requirements for the success of fuel cell vehicles. Efficient fuel cell system power production depends on proper air and hydrogen feed, and heat and water management. During transients, the fuel cell stack breathing control system is required to maintain proper temperature, membrane hydration, and partial pressure of the reactants across the membrane to avoid degradation of the stack voltage, and to maintain high efficiency and long stack life [1]. Creating a control-oriented model is a critical first step for the understanding of the system behavior, and the subsequent design and analysis of model-based control systems

Models suitable for control studies have certain attributes. Important characteristics such as dynamic (transient) effects are included while effects such as spatial variation of parameters or dynamic variables are discretized, lumped, or ignored. In this paper, only dynamic effects that are related to automobile operations are included in the model. The extremely fast electrochemical reactions and electrical dynamics have minimal effects on automobile applications and thus are neglected. The transient behavior due to manifold filling dynamics, membrane water content, supercharging devices, and temperature may impact the behavior of the vehicle [2], and should be included in the model. However, since the stack temperature is much slower compared with other dynamic phenomena, it could be simulated and regulated with its own (slower) controller. The temperature is thus treated as a parameter in the model.

Despite a large number of publications on fuel cell modeling, relatively few are suitable for control studies. Many publications target the fuel cell performance prediction with the main purpose of designing cell components and choosing fuel cell operating points [3–6]. These models are mostly steady-state, analyzed at the cell level, and include spatial variations of fuel cell parameters. They usually focus on electrochemistry, thermodynamics and fluid mechanics. These models are not suitable for control studies. However, they do provide useful knowledge about the operation of fuel cell stacks. On the other end of the spectrum, many steady-state system models were developed for component sizing [7,8], and cumulative fuel consumption or hybridization studies [9–11]. Here, the compressor, heat exchanger and fuel cell stack voltage are represented by look-up tables or efficiency maps. Usually, the only dynamics considered in this type of models is the vehicle inertia, and sometimes fuel cell stack temperature. The temperature dynamic is the focus of several publications [12–14]. Many of these papers focus on the startup period, during which the stack operating temperature needs to be reached quickly. A few publications [2,15,16] include the dynamics of the air supply system and their influence on the fuel cell system behavior.

In this paper, a dynamic fuel cell system model suitable for control studies is presented. The transient phenomena captured in the model include the flow and inertia dynamics of the compressor, the manifold filling dynamics (both anode and cathode), and membrane humidity. These variables affect the fuel cell stack voltage, and thus fuel cell efficiency and power. Unlike other models in the literature where a single polarization curve or a set of polarization curves under different cathode pressure is used, the fuel cell polarization curve used in this paper is a function of oxygen and hydrogen partial pressure, stack temperature, and membrane water content. This allows us to assess the effects of varying oxygen concentration and membrane humidity on the fuel cell voltage, which is necessary for control development during transient operation.

The current status of the fuel cell industry and research is highly secretive. Therefore, we are not able to obtain test data to completely verify our model. The main contribution of this paper is thus in compiling the scattered information in the literature, and constructing a model template to reflect the state of the art. The obtained model is useful in showing the behavior of fuel cell systems qualitatively, rather than quantitatively.
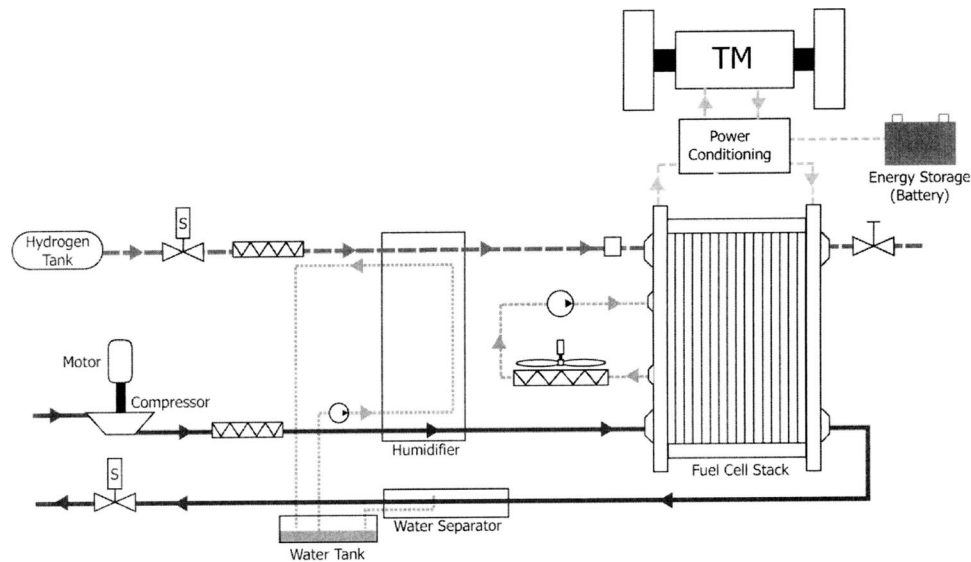

Fig. 1 Automotive fuel cell propulsion system

2 Fuel Cell Propulsion System for Automobiles

A fuel cell stack needs to be integrated with several auxiliary components to form a complete fuel cell system. The diagram in Fig. 1 shows an example fuel cell system. The fuel cell stack is augmented by four auxiliary systems: (i) hydrogen supply system, (ii) air supply system, (iii) cooling system, and (iv) humidification system. In Fig. 1, we assume that a compressed hydrogen tank is used. The control of hydrogen flow is thus achieved simply by controlling the hydrogen supply valve to reach the desired flow or pressure. The air is assumed to be supplied by an air compressor, which is used to increase the power density of the overall system. Figure 1 shows an external humidification system for both anode and cathode gases. PEM fuel cells without any external humidification have also been studied (e.g., [4]). Special membranes can be used in "self-humidification" designs [17]. In contrast to these other methods, external humidification usually provides higher authority and better performance, albeit at higher system complexity and cost.

The power of the fuel cell stack is a function of the current drawn from the stack and the resulting stack voltage. The cell voltage is a function of the stack current, reactant partial pressure inside each cell, cell temperature and membrane humidity. In this paper, we assume that the stack is well designed so that all cells perform similarly and can be lumped as a stack. For example, all the cell temperatures are identical, and thus we only need to keep track of the stack temperature; if starvation or membrane dehydration exists, it occurs simultaneously in every cell and thus all cells are represented by the same set of polarization curves. This assumption of invariable cell-to-cell performance is necessary for low-order system models.

As electric current is drawn from the stack, oxygen and hydrogen are consumed, and water and heat are generated. To maintain the desired hydrogen partial pressure, the hydrogen needs to be replenished by its supply system, which includes the pressurized hydrogen tank and a supply servo valve. Similarly, the air supply system needs to replenish the air to maintain the oxygen partial pressure. The air supply system consists of an air compressor, an electric motor and pipes or manifolds between the components. The compressor not only achieves desired air flow but also increases air pressure which significantly improves the reaction rate at the membranes, and thus the overall efficiency and power density. Since the pressurized air flow leaving the compressor is at a higher temperature, an air cooler may be needed to reduce the temperature of the air entering the stack. A humidifier is used to

prevent dehydration of the fuel cell membrane. The water used in the humidifier is supplied from the water tank. Water level in the tank is maintained by collecting water generated in the stack, which is carried out with the air flow. The excessive heat released in the fuel cell reaction is removed by the cooling system, which circulates deionized water through the fuel cell stack and removes the excess heat via a heat exchanger. Power conditioning is usually needed since the voltage of fuel cell stack varies significantly.

3 Fuel Cell System Model

In this paper, we will not present a model that includes all sub-systems shown in Fig. 1. Rather, the problem is simplified by assuming that the stack temperature is constant. This assumption is justified because the stack temperature changes relatively slowly, compared with the ~100 ms transient dynamics included in the model to be developed. Additionally, it is also assumed that the temperature and humidity of the inlet reactant flows are perfectly controlled, e.g., by well designed humidity and cooling sub-systems.

The system studied in this paper is shown in Fig. 2. It is assumed that the cathode and anode volumes of the multiple fuel cells are lumped as a single stack cathode and anode volumes. The anode supply and return manifold volumes are small, which al-
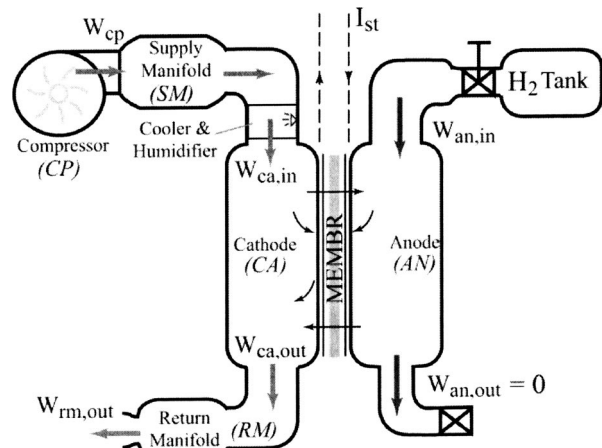

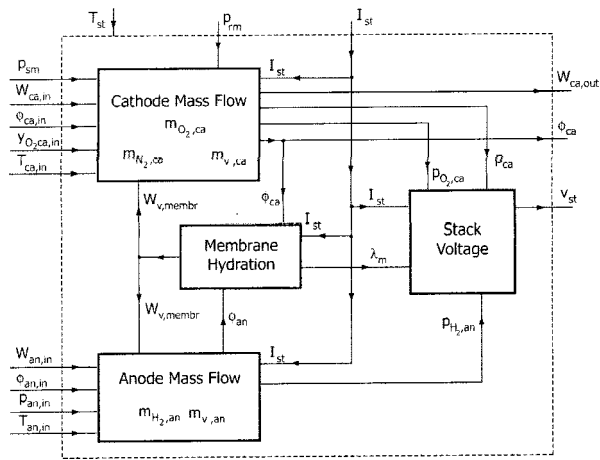**Fig. 2 Simplified fuel cell reactant supply system**

Fig. 3 Fuel cell stack block diagram

Fig. 4 Fuel cell polarization curve fitting results at 80°

lows us to lump these volumes to one "anode" volume. We denote all the variables associated with the lumped anode volume with a subscript (an). The cathode supply manifold (sm) lumps all the volumes associated with pipes and connection between the compressor and the stack cathode (ca) flow field. The cathode return manifold (rm) represents the lumped volume of pipes downstream of the stack cathode. In this paper, an expander is not included; however, one will be added in future models. It is assumed that the properties of the flow exiting a volume are the same as those of the gas inside the volume. Subscripts (cp) and (cm) denote variables associated with the compressor and compressor motor, respectively.

The rotational dynamics and a flow map are used to model the compressor. The law of conservation of mass is used to track the gas species in each volume. The principle of mass conservation is applied to calculate the properties of the combined gas in the supply and return manifolds. The law of conservation of energy is applied to the air in the supply manifold to account for the effect of temperature variations. The model is developed primarily based on physics. However, several phenomena are described in empirical equations. In the following sections, models for the fuel cell stack, compressor, manifolds, air cooler and humidifier are presented.

3.1 Fuel Cell Stack Model. The electrochemical reaction at the membranes is assumed to occur instantaneously. The fuel cell stack (st) model contains four interacting sub-models: the stack voltage model, the anode flow model, the cathode flow model, and the membrane hydration model (Fig. 3). We assume that the stack temperature is constant at 80°C. The voltage model contains an equation to calculate stack voltage based on fuel cell pressure, temperature, reactant gas partial pressures and membrane humidity. The dynamically varying pressure and relative humidity of the reactant gas flow inside the stack flow channels are calculated in the cathode and the anode flow models. The process of water transfer across the membrane is governed by the membrane hydration model. These subsystem models are discussed in the following sub-sections.

3.1.1 Stack Voltage Model. The stack voltage is calculated as a function of stack current, cathode pressure, reactant partial pressures, fuel cell temperature and membrane humidity. The current-voltage relationship is commonly given in the form of the polarization curve, which is plotted as cell voltage, v_{fc}, versus cell current density, i_{fc} (see Fig. 4 for an example). Since the fuel cell stack consists of multiple fuel cells connected in series, the stack voltage, v_{st}, is obtained as the sum of the individual cell voltages; and the stack current, I_{st}, is equal to the cell current. The current density is then defined as stack current per unit of cell
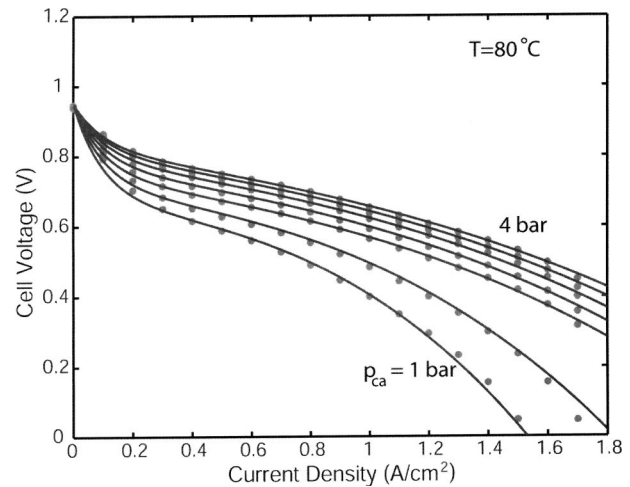
active area, $i_{fc} = I_{st}/A_{fc}$. Under the assumption that all cells are identical, the stack voltage can be calculated by multiplying the cell voltage, v_{fc}, by the number of cells, n, of the stack ($v_{st} = n \times v_{fc}$).

The fuel cell voltage is calculated using a combination of physical and empirical relationships, and is given by [18]

$$v_{fc} = E - v_{act} - v_{ohm} - v_{conc} \qquad (1)$$

where E is the open circuit voltage and v_{act}, v_{ohm} and v_{conc} are activation, ohmic and concentration overvoltages, which represent losses due to various physical or chemical factors. The open circuit voltage is calculated from the energy balance between the reactants and products, and the Faraday Constant, and is [3]

$$E = 1.229 - 8.5 \times 10^{-4}(T_{fc} - 298.15)$$
$$+ 4.3085 \times 10^{-5} T_{fc} \left[\ln(p_{H_2}) + \frac{1}{2}\ln(p_{O_2}) \right] \quad \text{(Volts)} \quad (2)$$

where the fuel cell temperature T_{fc} is expressed in Kelvin, and reactant partial pressures p_{H_2} and p_{O_2} are expressed in atm.

The activation overvoltage, v_{act}, arises from the need to move electrons and to break and form chemical bonds at the anode and cathode [19]. The relationship between the activation overvoltage and the current density is described by the Tafel equation, which is approximated by

$$v_{act} = v_0 + v_a (1 - e^{-c_1 i}) \qquad (3)$$

The activation overvoltage depends on temperature and oxygen partial pressure [3,20]. The values of v_0, v_a and c_1 and their dependency on oxygen partial pressure and temperature can be determined from nonlinear regression of experimental data.

The ohmic overvoltage, v_{ohm}, arises from the resistance of the polymer membrane to the transfer of protons and the resistance of the electrodes and collector plates to the transfer of electrons. The voltage drop is thus proportional to the stack current

$$v_{ohm} = i \cdot R_{ohm} \qquad (4)$$

The resistance, R_{ohm}, depends strongly on membrane humidity [21] and cell temperature [22]. The ohmic resistance is proportional to membrane thickness t_m and inversely proportional to the membrane conductivity, $\sigma_m(\lambda_m, T_{fc})$ $(\Omega \cdot cm)^{-1}$ [6,23], i.e.,

$$R_{ohm} = \frac{t_m}{\sigma_m} \qquad (5)$$

where λ_m represents the membrane water content. The membrane conductivity is a function of membrane humidity and temperature in the form [6]

$$\sigma_m = (b_{11}\lambda_m - b_{12})\exp\left(b_2\left(\frac{1}{303} - \frac{1}{T_{fc}}\right)\right) \qquad (6)$$

where the value of t_m, b_{11} and b_{12} for the Nafion 117 membrane [6] are used, and b_2 is adjusted to fit our fuel cell data. The calculation of λ_m is given in Section 4.1.4. Its value varies between 0 and 14 [6], which correspond to relative humidity (RH) of 0% and 100%, respectively [23].

The concentration overvoltage, v_{conc}, results from the increased loss at high current density, e.g., a significant drop in reactant concentration due to both high reactant consumption and head loss at high flow rate. This term is ignored in some models, e.g., [24], perhaps because it is not desirable to operate the stack at regions where v_{conc} is high (efficiency is low). If the stack will operate at high current density, however, this term needs to be included. An equation to approximate the concentration losses is given by [2]

$$v_{conc} = i\left(c_2 \frac{i}{i_{max}}\right)^{c_3} \qquad (7)$$

where c_2, c_3 and i_{max} are constants that depend on temperature and reactant partial pressure and can be determined empirically.

The coefficients in Equations (3) and (7) are determined using nonlinear regression with polarization data from an automotive propulsion-sized PEM fuel cell stack [1]. By assuming that the data is obtained from the fuel cell stack operating under a well-controlled environment, where cathode gas is fully humidified and oxygen excess ratio (ratio of oxygen supplied to oxygen reacted) is regulated at 2, the pressure terms in the activation and concentration overvoltage terms can be related to oxygen partial pressure, p_{O_2}, and vapor saturation pressure, p_{sat}. The regression results are

$$v_0 = 0.279 - 8.5\times10^{-4}(T_{fc} - 298.15) + 4.3085\times10^{-5}T_{fc}\left[\ln\left(\frac{p_{ca} - p_{sat}}{1.01325}\right) + \frac{1}{2}\ln\left(\frac{0.1173(p_{ca} - p_{sat})}{1.01325}\right)\right]$$

$$v_a = (-1.618\times10^{-5}T_{fc} + 1.618\times10^{-2})\left(\frac{p_{O_2}}{0.1173} + p_{sat}\right)^2 + (1.8\times10^{-4}T_{fc} - 0.166)\left(\frac{p_{O_2}}{0.1173} + p_{sat}\right)$$

$$\quad + (-5.8\times10^{-4}T_{fc} + 0.5736)$$

$$c_1 = 10, \quad c_3 = 2, \quad i_{max} = 2.2$$

$$b_{11} = 0.05139, \quad b_{12} = 0.00326, \quad b_2 = 350$$

$$c_2 = \begin{cases} (7.16\times10^{-4}T_{fc} - 0.622)\left(\frac{p_{O_2}}{0.1173} + p_{sat}\right) + (-1.45\times10^{-3}T_{fc} + 1.68), & \text{if } \frac{p_{O_2}}{0.1173} + p_{sat} < 2 \text{ atm} \\ (8.66\times10^{-5}T_{fc} - 0.068)\left(\frac{p_{O_2}}{0.1173} + p_{sat}\right) + (-1.6\times10^{-4}T_{fc} + 0.54), & \text{else} \end{cases} \qquad (8)$$

The predicted voltage and experimental data for $T_{fc} = 80°C$ and various cathode pressure is shown in Fig. 4. Results at other temperatures (between 40°C and 100°C) all have similar accuracy. Based on the stack model developed above, the effect of membrane water content on cell voltage is illustrated in Fig. 5, which
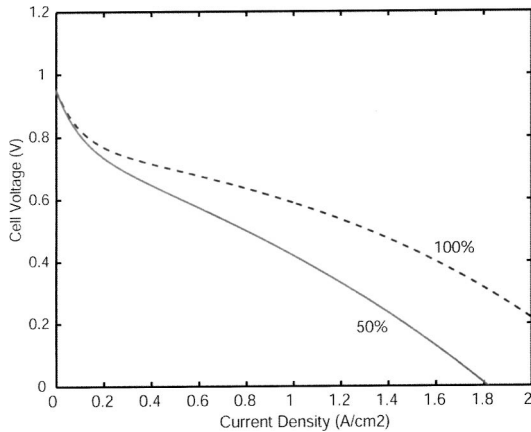
Fig. 5 Effect of membrane water content (100°C and 2.5 bar air pressure)

shows fuel cell polarization curves for a membrane water content at 100% and 50%. The model predicts significant reduction in fuel cell voltage due to change in the membrane water content, which illustrates the importance of humidity control. It should be noted that oversaturated (flooding) conditions will cause condensation and liquid formation inside the anode or the cathode, which leads to voltage degradation [25]. This effect is currently not captured in our model. Note also that the coefficients in Equation (8) are derived from experimental data for a specific stack. To model a different stack, the same basis functions in Equations (2)–(7) may be used but the coefficients need to be determined using data from the new stack.

3.1.2 Cathode Flow Model. This model captures the cathode air flow behavior, and is developed using the mass conservation principle and the thermodynamic and psychrometric properties of air. Several assumptions are made: (1) All gases obey the ideal gas law; (2) The temperature of the air inside the cathode is equal to the stack temperature; (3) The properties of the flow exiting the cathode such as temperature, pressure, and humidity are assumed to be the same as those inside the cathode; (4) When the relative humidity of the gas exceeds 100%, vapor condenses into the liquid form. The liquid water does not leave the stack and will either evaporate when the humidity drops below 100% or accumulate in the cathode; (5) finally, the flow channel and cathode backing layer are lumped into one volume, i.e., the spatial variations are
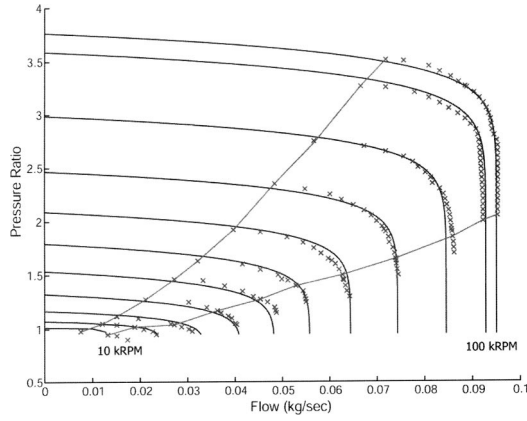
Fig. 6 Cathode flow model

ignored. The mass continuity is used to balance the mass of the three elements—oxygen, nitrogen and water, inside the cathode volume.

$$\frac{dm_{O_2}}{dt} = W_{O_2,in} - W_{O_2,out} - W_{O_2,reacted}$$

$$\frac{dm_{N_2}}{dt} = W_{N_2,in} - W_{N_2,out}$$

$$\frac{dm_{w,ca}}{dt} = W_{v,ca,in} - W_{v,ca,in} - W_{v,ca,out} + W_{v,ca,gen} + W_{v,membr}$$

$$(9)$$

Using the masses of oxygen, m_{O_2}, nitrogen, m_{N_2}, and water, m_w, and the stack temperature, T_{st}, we use the ideal gas law and thermodynamic properties to calculate oxygen, nitrogen and vapor partial pressure, p_{O_2}, p_{N_2}, $p_{v,ca}$, cathode total pressure, $p_{ca} = p_{O_2} + p_{N_2} + p_{v,ca}$, relative humidity, ϕ_{ca}, and dry air oxygen mole fraction, $y_{O_2,ca}$, of the cathode flow. If the calculated water mass is more than that of the saturated state, the extra amount is assumed to condense to liquid form instantaneously. Figure 6 illustrates the cathode model in a block diagram format.

The inlet (in) and outlet (out) mass flow rate of oxygen, nitrogen and vapor in Equation (9) are calculated from the inlet and outlet cathode flow conditions using thermodynamic properties. The detailed calculations are given in Appendices A and B. The cathode inlet flow rate and condition are calculated in the humidifier model (Section 4.5). A linearized nozzle equation (A4) is used to calculate the cathode exit flow rate, $W_{ca,out}$. Electrochemistry principles are used to calculate the rates of oxygen consumption, $W_{O_2,reacted}$, and water production, $W_{v,ca,gen}$, from the stack current I_{st}:

$$W_{O_2,reacted} = M_{O_2} \times \frac{nI_{st}}{4F} \tag{10}$$

$$W_{v,ca,gen} = M_v \times \frac{nI_{st}}{2F} \tag{11}$$

where F is the Faraday Constant ($=96485$ Coulombs) and M_{O_2} and M_v are the molar masses of oxygen and water, respectively. The water flow rate across the membrane, $W_{v,membr}$, in Equation (9) is calculated from the membrane hydration model in Section 4.1.4.

3.1.3 Anode Flow Model. This model is quite similar to the cathode flow model. Hydrogen partial pressure and anode flow humidity are determined by balancing the mass of hydrogen, m_{H_2}, and water in the anode, $m_{w,an}$.

$$\frac{dm_{H_2}}{dt} = W_{H_2,in} - W_{H_2,out} - W_{H_2,reacted} \tag{12}$$

$$\frac{dm_{w,an}}{dt} = W_{v,an,in} - W_{v,an,out} - W_{v,membr} \tag{13}$$

In this model, pure hydrogen gas is assumed to be supplied to the anode from a hydrogen tank. It is assumed that the hydrogen flow rate can be instantaneously adjusted by a valve while maintaining a minimum pressure difference across the membrane. This has been achieved by using a high gain proportional controller, discussed in Section 4.7, to control the hydrogen flow rate such that the anode pressure, p_{an}, tracks the cathode pressure, p_{ca}. The inlet hydrogen flow is assumed to have 100% relative humidity. The anode outlet flow represents possible hydrogen purge and is currently assumed to be 0 ($W_{an,out} = 0$). The anode hydrogen temperature is assumed to be equal to the stack temperature. The rate of hydrogen consumed in the reaction, $W_{H_2,reacted}$, is a function of the stack current

$$W_{H_2,reacted} = M_{H_2} \times \frac{nI_{st}}{2F} \tag{14}$$

where M_{H_2} is hydrogen molar mass.

3.1.4 Membrane Hydration Model. The membrane hydration model captures the effect of water transport across the membrane. Both water content and mass flow are assumed to be uniform over the surface area of the membrane, and are functions of stack current and relative humidity of the gas in the anode and cathode.

The water transport across the membrane is achieved through two distinct phenomena [6,23]. First, the electro-osmotic drag phenomenon is due to the water molecules dragged across the membrane from anode to cathode by the protons. The amount of water transported is proportional to the electro-osmotic drag coefficient, n_d, which is defined as the number of water molecules carried by each proton. Secondly, the gradient of water concentration across the membrane results in "back-diffusion" of water, usually from cathode to anode [26]. The water concentration, c_v, is assumed to change linearly over the membrane thickness, t_m. Combining the two water transport mechanisms, the water flow across the membrane from anode to cathode is

$$W_{v,membr} = M_v A_{fc} n \left(\frac{n_d I_{st}}{F} - D_w \frac{c_{v,ca} - c_{v,an}}{t_m} \right) \tag{15}$$

The coefficients n_d and D_w vary with membrane water content, λ_m, which is calculated from the average of the water content at the anode (λ_{an}) and cathode (λ_{ca}). λ_{an} and λ_{ca} are calculated from the membrane water activity, $a_i = y_{v,i} p_i / p_{sat,i} = p_{v,i} / p_{sat,i}$: $i \in [an, ca]$, from the following equation:

$$\lambda_i = \begin{cases} 0.043 + 17.81 a_i - 39.85 a_i^2 + 36 a_i^3, & 0 < a_i \leq 1 \\ 14 + 1.4(a_i - 1), & 1 < a_i \leq 3 \end{cases} \tag{16}$$

The electro-osmotic and diffusion coefficients are calculated from [26]

$$n_d = 0.0029 \lambda_m^2 + 0.05 \lambda_m - 3.4 \times 10^{-19} \tag{17}$$

and

$$D_w = D_\lambda \exp \left(2416 \left(\frac{1}{303} - \frac{1}{T_{fc}} \right) \right) \tag{18}$$

where

Fig. 7 Compressor map

$$D_\lambda = \begin{cases} 10^{-6}, & \lambda_m < 2 \\ 10^{-6}(1+2(\lambda_m-2)), & 2 \le \lambda_m < 3 \\ 10^{-6}(3-1.67(\lambda_m-3)), & 3 \le \lambda_m < 4.5 \\ 1.25 \times 10^{-6}, & \lambda_m \ge 4.5 \end{cases} \qquad (19)$$

and T_{fc} is the fuel cell temperature. The water concentration at the membrane surfaces, $c_{v,ca}$ and $c_{v,an}$, are functions of water content on the surface, λ_{ca} and λ_{an}. Specifically, $c_{v,i} = \rho_{m,dry}\lambda_i/M_{m,dry}$, $i \in [an,ca]$ where $\rho_{m,dry}$ (kg/cm^3) is the dry membrane density and $M_{m,dry}$ (kg/mol) is the membrane dry equivalent weight. These equations are developed based on experimental results measured for Nafion 117 membrane in [6]. During the last decade, PEM membranes have evolved tremendously and the empirical Equations (16)–(19) may no longer be a good representation of the new membrane properties. However, information about newer membranes is not available in the literature at the time this paper is written.

3.2 Compressor Model. A lumped rotational model is used to represent the dynamic behavior of the compressor,

$$J_{cp}\frac{d\omega_{cp}}{dt} = \tau_{cm} - \tau_{cp} \qquad (20)$$

where $\tau_{cm}(v_{cm}, \omega_{cp})$ is the compressor motor (CM) torque and τ_{cp} is the load torque to be explained below. The compressor motor torque is calculated using a static motor equation

$$\tau_{cm} = \eta_{cm}\frac{k_t}{R_{cm}}(v_{cm} - k_v\omega_{cp}) \qquad (21)$$

where k_t, R_{cm} and k_v are motor constants and η_{cm} is the motor mechanical efficiency. The torque required to drive the compressor is calculated using the thermodynamic equation

$$\tau_{cp} = \frac{C_p}{\omega_{cp}}\frac{T_{atm}}{\eta_{cp}}\left[\left(\frac{p_{sm}}{p_{atm}}\right)^{(\gamma-1)/\gamma} - 1\right]W_{cp} \qquad (22)$$

where γ is the ratio of the specific heats of air ($=1.4$), C_p is the constant-pressure specific heat capacity of air ($=1004$ J·kg^{-1}·K^{-1}), η_{cp} is compressor efficiency, p_{sm} is the pressure inside the supply manifold and p_{atm} and T_{atm} are the atmospheric pressure and temperature, respectively.

A static compressor map is used to determine the air flow rate through the compressor, W_{cp}. The compressor flow characteristic $W_{cp}(p_{sm}/p_{atm}, \omega_{cp})$ is modeled by the Jensen and Kristensen nonlinear curve fitting method [27], which represents the compressor data very well as shown in Fig. 7. The compressor model used here is for an Allied Signal compressor [28]. Thermodynamic equations are used to calculate the exit air temperature.

$$T_{cp} = T_{atm} + \frac{T_{atm}}{\eta_{cp}}\left[\left(\frac{p_{sm}}{p_{atm}}\right)^{(\gamma-1)/\gamma} - 1\right] \qquad (23)$$

3.3 Supply Manifold Model. The cathode supply manifold (SM) includes pipe and stack manifold volumes between the compressor and the fuel cells. The supply manifold pressure, p_{sm}, is governed by mass continuity and energy conservation equations

$$\frac{dm_{sm}}{dt} = W_{cp} - W_{sm,out} \qquad (24)$$

$$\frac{dp_{sm}}{dt} = \frac{\gamma R_a}{V_{sm}}(W_{cp}T_{cp} - W_{sm,out}T_{sm}) \qquad (25)$$

where R_a is the air gas constant, V_{sm} is the supply manifold volume, and T_{sm} is the temperature of the flow inside the manifold calculated from the ideal gas law. The supply manifold exit flow, $W_{sm,out}$, is calculated as a function of p_{sm} and p_{ca} using the linearized nozzle flow equation shown in Appendix A.

3.4 Static Air Cooler Model. The air temperature leaving the compressor is usually high due to the increased pressure. To prevent the fuel cell membrane from damaging, the air may need to be cooled down before it is sent to the stack. In this study, we assume that an ideal air cooler (CL) maintains the temperature of the air entering the stack at $T_{cl} = 80°$C. Further, it is assumed that the pressure drop across the cooler is negligible, $p_{cl} = p_{sm}$. The humidity of the gas exiting the cooler is then calculated from

$$\phi_{cl} = \frac{P_{v,cl}}{p_{sat}(T_{cl})} = \frac{p_{cl}p_{v,atm}}{p_{atm}p_{sat}(T_{cl})} = \frac{p_{cl}\phi_{atm}p_{sat}(T_{atm})}{p_{atm}p_{sat}(T_{cl})} \qquad (26)$$

where $\phi_{atm} = 0.5$ is the assumed ambient air relative humidity and $p_{sat}(\square)$ is the vapor saturation pressure.

3.5 Static Humidifier Model. Since we assume that the inlet air is humidified to the desired relative humidity before entering the stack, a static humidifier model is needed to calculate the required water that needs to be injected into the air. Additionally, the model also determines the changes in total flow rate and pressure due to the added water. The temperature of the flow is assumed constant. The water injected is assumed to be in the form of vapor. The amount of vapor injected is calculated from the vapor flow at the cooler outlet and the required vapor flow for the desired humidity, ϕ_{des}. Based on the condition of the flow exiting the cooler $W_{cl}(W_{sm,out}, p_{cl}, T_{cl}, \phi_{cl})$, the dry air mass flow rate, $W_{a,cl}$, the vapor mass flow rate, $W_{v,cl}$, and the dry air pressure, $p_{a,cl}$, are calculated using Equations (B1)–(B5). The flow rate of vapor injected is then calculated from

$$W_{v,inj} = \frac{M_v}{M_a}\frac{\phi_{des}p_{sat}(T_{cl})}{p_{a,cl}}W_{a,cl} - W_{v,cl} \qquad (27)$$

where M_v and M_a are molar mass of vapor and dry air, respectively. The cathode inlet flow rate and pressure are $W_{ca,in} = W_{cl} + W_{v,inj}$ and $p_{ca,in} = p_{a,cl} + \phi_{des}p_{sat}(T_{cl})$.

3.6 Return Manifold Model. Unlike the supply manifold, where temperature changes need to be considered, the temperature in the return manifold, T_{rm}, is assumed constant and equal to the temperature of the flow leaving the cathode. The return manifold pressure, p_{rm}, is governed by the mass conservation and the ideal gas law through isothermal assumptions.

$$\frac{dp_{rm}}{dt} = \frac{R_a T_{rm}}{V_{rm}}(W_{ca,out} - W_{rm,out}) \qquad (28)$$

The nonlinear nozzle equations (A2)–(A3) are used to calculate the return manifold exit air flow rate, $W_{rm,out}$, as a function of the return manifold pressure and back-pressure valve opening area, $A_{T,rm}$.

Table 1 Model parameters for vehicle-size fuel cell system

Symbol	Variable	Value
$\rho_{m,dry}$	Membrane dry density	0.002 kg/cm^3
$M_{m,dry}$	Membrane dry equivalent weight	1.1 kg/mol
t_m	Membrane thickness	0.01275 cm
n	Number of cells in stack	381
A_{fc}	Fuel cell active area	280 cm^2
d_c	Compressor diameter	0.2286 m
J_{cp}	Compressor and motor inertia	5×10^{-5} kg·m^2
V_{an}	Anode volume	0.005 m^3
V_{ca}	Cathode volume	0.01 m^3
V_{sm}	Supply manifold volume	0.02 m^3
V_{rm}	Return manifold volume	0.005 m^3
$C_{D,rm}$	Return manifold throttle discharge coefficient	0.0124
$A_{T,rm}$	Return manifold throttle area	0.002 m^2
$k_{sm,out}$	Supply manifold outlet orifice constant	0.3629×10^{-5} kg/(s·Pa)
$k_{ca,out}$	Cathode outlet orifice constant	0.2177×10^{-5} kg(s·Pa)
k_v	Motor electric constant	0.0153 V/(rad/s)
k_t	Motor torque constant	0.0153 N-m/A
R_{cm}	Compressor Motor circuit resistance	0.816 Ω
η_{cm}	Compressor Motor efficiency	98%

3.7 Hydrogen Flow. Since pressurized hydrogen is used, the anode hydrogen flow can be regulated by a servo valve to achieve very high loop bandwidth. The goal of the hydrogen flow control is to minimize the pressure difference across the membrane, i.e., the difference between anode and cathode pressures. Since the valve is fast, it is assumed that the flow rate of hydrogen can be directly controlled based on the feedback of the pressure difference.

$$W_{an,in} = K_1(K_2 p_{sm} - p_{an}) \qquad (29)$$

where $K_1 = 2.1$ kg/s/kPa is the proportional gain and $K_2 = 0.94$ takes into account a nominal pressure drop between the supply manifold and the cathode. A purge valve is commonly installed at the anode exit to remove water droplets. The purge valve can be used to reduce the anode pressure quickly if necessary (e.g., when anode flow calculated from Equation (29) is negative).

3.8 Model Summary. The fuel cell system model developed above contains nine states. The compressor has one state: rotor speed. The supply manifold has two states: air mass and air pressure. The return manifold has one state: air pressure. The stack has five states: O_2, N_2, and vapor masses in the cathode, and H_2 and vapor masses in the anode. These states then determine the voltage output of the stack. Under the assumptions of a perfect humidifier and air cooler, and the use of proportional control of the hydrogen valve, the only inputs to the model are the stack current, I_{st}, and the compressor motor voltage, v_{cm}. The parameters used in the model are given in Table 1. Most of the parameters are based on the 75 kW stacks used in the FORD P2000 fuel cell prototype vehicle [29]. The active area of the fuel cell is calculated from the peak power of the stack. The values of the volumes are approximated from the dimensions of the P2000 fuel cell system.

4 Steady-State Analysis

The model we have developed will be used to conduct a few example analyses important to fuel cell system engineers. In this section, the optimal steady-state operating point for the air compressor is studied. The net power of the fuel cell system, P_{net}, which is the difference between the power produced by the stack, P_{st}, and the parasitic power, should be maximized. The majority of the parasitic power for an automotive fuel cell system is spent on the air compressor, thus, it is important to determine the proper air flow. The air flow excess is reflected by the term oxygen excess ratio, λ_{O_2}, defined as the ratio of oxygen supplied to oxygen used in the cathode, i.e.,

$$\lambda_{O_2} = \frac{W_{O_2,in}}{W_{O_2,react}} \qquad (30)$$

High oxygen excess ratio, and thus high oxygen partial pressure, improves P_{st} and P_{net}. After an optimum value is reached, however, further increase in λ_{O_2} will result in an increase in compressor power and only marginal increase in P_{st}. Therefore, P_{net} decreases. To identify the optimal value for λ_{O_2}, we run the model repeatedly, and then plot steady-state values of λ_{O_2} and P_{net}, at different stack current I_{st} (see Fig. 8). It can be seen that the optimal oxygen excess ratio varies between 2.0 and 2.4, and de-
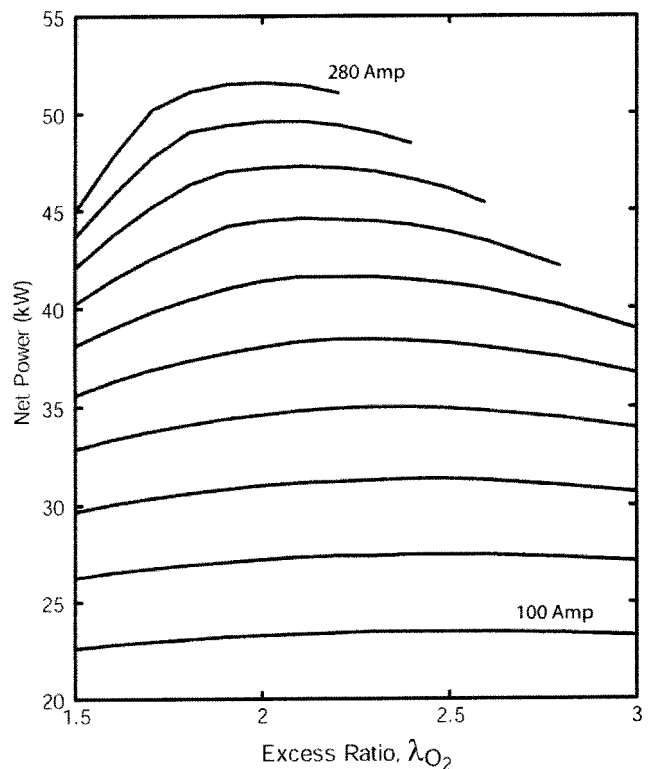
Fig. 8 System net power at different stack current and oxygen excess ratios
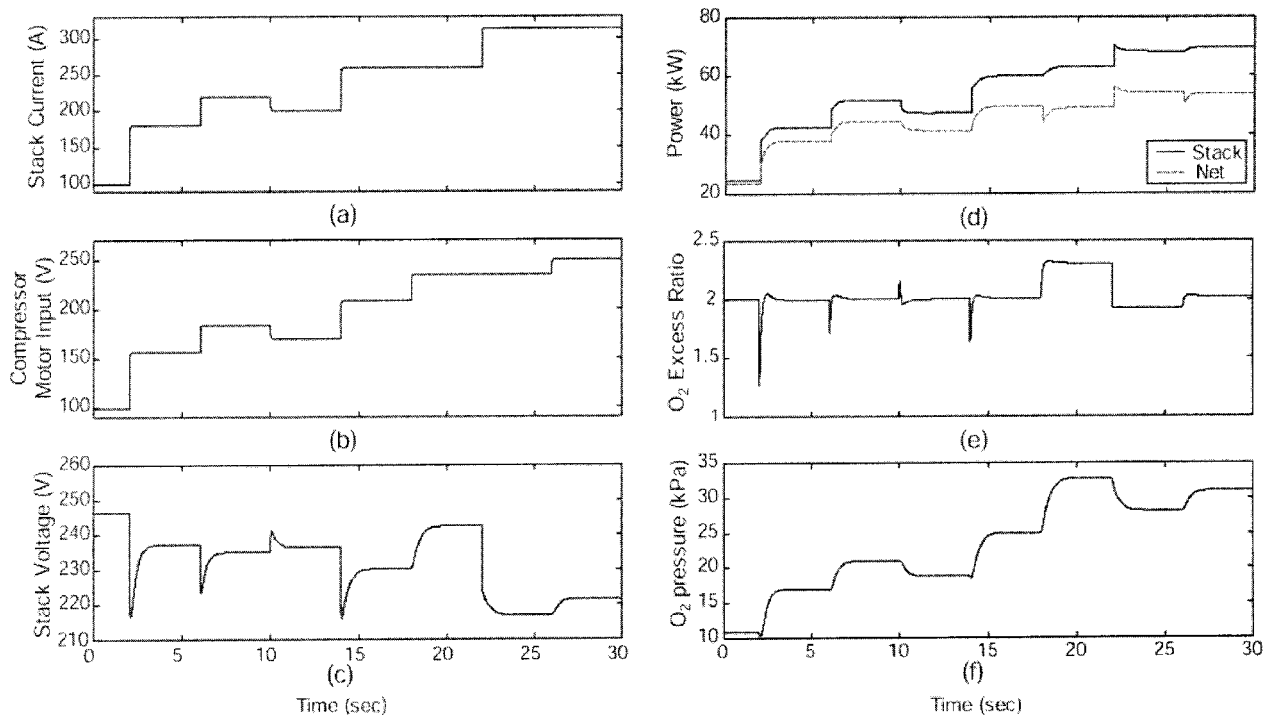
Fig. 9 Simulation results of the fuel cell system model for a series of input step changes

creases slowly when the stack current increases. Note that the results may also be influenced by factors not included in the model, such as stack flooding.

5 Dynamic Simulation

A series of step changes in stack current (Fig. 9(a)) and compressor motor input voltage (Fig. 9(b)) are applied to the stack at a nominal stack operating temperature of 80°C. During the first four steps, the compressor voltage is controlled so that the optimal oxygen excess ratio (~2.0) is maintained. This is achieved with the simple static feedforward controller as shown in Fig. 10. The remaining steps are then applied independently, resulting in different levels of oxygen excess ratios (Figure 9(e)).

During a positive current step, the oxygen excess ratio drops due to the depletion of oxygen (Fig. 9(e)), which causes a significant drop in the stack voltage (Fig. 9(c)). When the compressor voltage is controlled by the feedforward algorithm, there is still a noticeable transient effect on the stack voltage (Fig. 9(c)), and oxygen partial pressure at cathode exit (Fig. 9(f)). The step at t = 18 seconds shows the response of giving a step increase in the compressor input while keeping constant stack current. An opposite case is shown at t = 22 s. The response between 18 and 22 s shows the effect of running the system at an excess ratio higher

than the optimum value. It can be seen that even though the stack voltage (power) increases, the net power actually decreases due to the increased parasitic loss.

Figure 11 shows the fuel cell response described above plotted on the polarization map. The results are qualitatively similar to the experimental results presented in [21]. The compressor response for this simulation is shown in Fig. 12. The plot shows that the compressor response does not follow the operating line (dashed line) during transient. It is also clear from Figure 12 that large and rapid reductions of the compressor voltage should be avoided as the compressor may be pushed into the surge (instability) region [30].
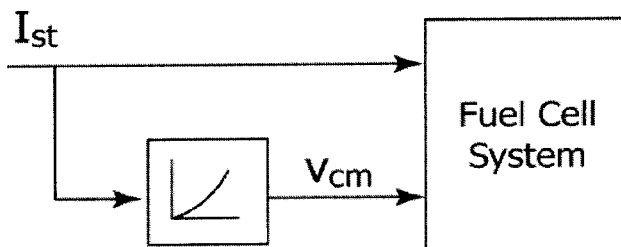

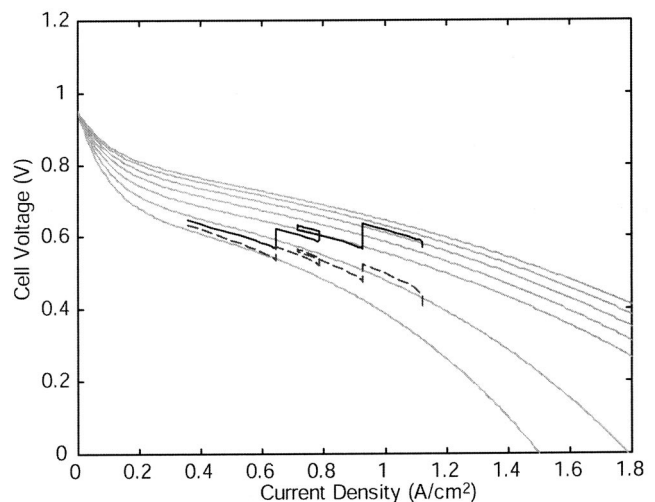**Fig. 10 Static feedforward using steady-state map**

Fig. 11 Fuel cell response on polarization curve. Solid line assumes fully humidified membrane; dashed line represents drying membrane.
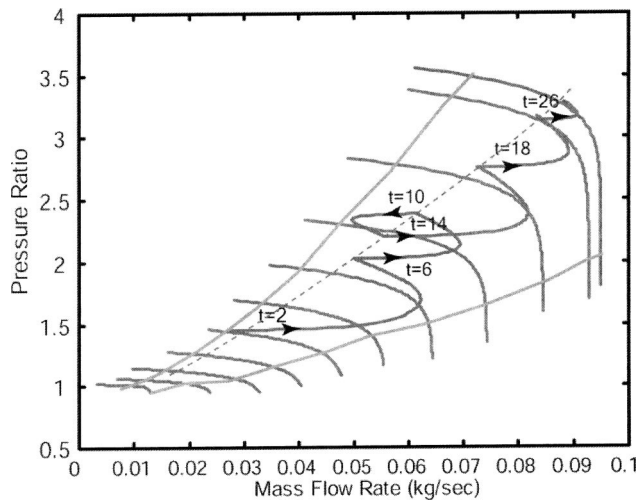
Fig. 12 Compressor transient response on compressor map

6 Observability Analysis

Simulation results in the previous section show that a static controller is not good enough in rejecting the adverse effect of disturbances (stack load current). The design of an advanced control algorithm is beyond the scope of this paper; however, we would like to present example analysis of the observability of different measurements, a critical step for multivariable control development. In this section, a linearized model will be used to study the system observability. Three measurements are investigated: compressor air flow rate, $y_1 = W_{cp}$, supply manifold pressure, $y_2 = p_{sm}$, and fuel cell stack voltage, $y_3 = V_{st}$. These signals are usually available because they are easy to measure and are useful for other purposes. For example, the compressor flow rate is typically measured for the internal feedback of the compressor. The stack voltage is monitored for diagnostics and fault detection purposes.

The LTI system analysis in MATLAB/SIMULINK control system toolbox is used to linearize the model. The nominal operating point is chosen to be $P_{net} = 40$ kW and $\lambda_{O_2} = 2$, which correspond to nominal inputs of $I_{st} = 191$ Amp and $v_{cm} = 164$ Volt. The linear model is

$$\dot{x} = Ax + Bu$$
$$y = Cx + Du \qquad (31)$$

where $x = [m_{O_2} \ m_{H_2} \ m_{N_2} \ \omega_{cp} \ p_{sm} \ m_{sm} \ m_{w,an} \ p_{rm}]^T$, $u = [v_{cm} \ I_{st}]^T$ and $y = [W_{cp} \ p_{sm} \ v_{st}]$. Here, the units of states and outputs are selected so that all variables have comparable magnitudes, and are as follows: mass in grams, pressure in bar, rotational speed in kRPM, mass flow rate in g/sec, power in kW, voltage in V, and current in A. The matrices of the linearized model in Equation (31) are given in Table 3.

The linear model has eight states while the nonlinear model has nine states. The state removed is the mass of water in the cathode. The reason is that the parameters of the membrane water flow available in the literature always predicts excessive water flow from anode to cathode which results in fully humidified cathode gas under all nominal conditions. Additionally, our nonlinear model does not include the effects of liquid condensation, also known as "flooding," on the fuel cell voltage response.

The analysis results on system observability are shown in Table 2. The table shows system eigenvalues, λ_i, eigenvectors, and corresponding rank and condition number of the matrix

$$\begin{bmatrix} \lambda_i I - A \\ C \end{bmatrix} \qquad (32)$$

for three different cases: 1) measuring only W_{cp} (y_1), 2) measuring W_{cp} and p_{sm} (y_1 and y_2), and 3) measuring all W_{cp}, p_{sm}, and v_{st} (all three outputs). The eigenvalue is unobservable if the corresponding matrix in Equation (32) loses rank [31]. A large condition number of a matrix implies that the matrix is almost rank deficient, i.e., the corresponding eigenvalue is weakly observable.

Table 2 shows that with only the compressor air flow rate W_{cp}, the system is not observable, and adding p_{sm} measurement does not change the observability. This is because pressure and flow are related by an integrator. The eigenvalues -219.63 and -22.404 are not observable with measurements W_{cp} and p_{sm}. The eigenvectors associated with these eigenvalues reveal that the unobservable mode is associated with the dynamics at the anode side. This analysis is consistent with intuition since these two measurements are on the air supply side and the only connection between them to the anode is through a weak membrane water transport. These two unobservable eigenvalues are, however, stable and fast, and thus they may only have a small effect on the estimation of other states. On the other hand, the slow eigenvalues at -1.6473 and -1.4038 can degrade estimator performance because they are weakly observable, as indicated by large condition number at 9728.4 and 2449.9, respectively.

Adding the stack voltage measurement substantially improves the state observability, as can be seen from the rank and the condition number for Case 3. Stack voltage is currently used for monitoring, diagnostic, and emergency stack shut-down proce-

Table 2 Eigenvalues, eigenvectors, and observability

Eigenvalues								
λ	−219.63	−89.485	−46.177	−22.404	−18.258	−2.915	−1.6473	−1.4038
Eigenvectors								
x1	1.06E−16	−0.17539	−0.091325	3.43E−16	0.050201	0.024367	0.86107	−0.25619
x2	0.29428	0.016479	0.012583	0.1289	0.0036888	0.016047	0.007579	−0.0074482
x3	−3.23E−16	−0.74707	−0.099392	−5.92E−16	0.13993	0.44336	−0.14727	−0.098068
x4	−1.21E−16	−0.12878	−0.45231	3.24E−15	−0.98678	0.62473	0.27811	−0.27037
x5	−9.58E−18	0.0479	0.067229	−5.98E−17	0.0046179	0.046501	0.022519	−0.022231
x6	−7.23E−17	0.61398	0.86233	−7.93E−16	0.057898	0.6389	0.3981	−0.92234
x7	0.95572	0.071474	0.11197	−0.99166	−0.016026	−0.0078755	−0.0026628	0.0024275
x8	−3.04E−17	0.099469	−0.12794	−2.05E−16	0.022705	0.043444	0.021407	−0.019503
measuring y1								
rank(λI-A; C)	7	8	8	7	8	8	8	8
cond(λI-A; C)	1.29E+16	171.17	157.79	9.52E+16	461.59	1130.3	9728.4	2449.9
measuring y1 y2								
rank(λI-A; C)	7	8	8	7	8	8	8	8
cond(λI-A; C)	1.32E+16	171.16	157.79	3.15E+17	461.59	1130.3	9728.4	2449.9
measuring y1 y2 y3								
rank(λI-A; C)	8	8	8	8	8	8	8	8
cond(λI-A; C)	226.69	154.99	143.86	943.77	402.8	938.86	1617	1886.2

Table 3 Linearized system matrices

A

$$
\begin{bmatrix}
-6.30908 & 0 & -10.9544 & 0 & 83.74458 & 0 & 0 & 24.05866 \\
0 & -161.083 & 0 & 0 & 51.52923 & 0 & -18.0261 & 0 \\
-18.7858 & 0 & -46.3136 & 0 & 275.6592 & 0 & 0 & 158.3741 \\
0 & 0 & 0 & -17.3506 & 193.9373 & 0 & 0 & 0 \\
1.299576 & 0 & 2.969317 & 0.3977 & -38.7024 & 0.105748 & 0 & 0 \\
16.64244 & 0 & 38.02522 & 5.066579 & -479.384 & 0 & 0 & 0 \\
0 & -450.386 & 0 & 0 & 142.2084 & 0 & -80.9472 & 0 \\
2.02257 & 0 & 4.621237 & 0 & 0 & 0 & 0 & -51.2108
\end{bmatrix}
$$

B

$$
\begin{bmatrix}
0 & 0 & -0.03159 \\
0 & 0 & -0.00398 \\
0 & 0 & 0 \\
0 & 3.946683 & 0 \\
0 & 0 & 0 \\
0 & 0 & 0 \\
0 & 0 & -0.05242 \\
0 & 0 & 0
\end{bmatrix}
$$

C

$$
\begin{bmatrix}
0 & 0 & 0 & 5.066579 & -116.446 & 0 & 0 & 0 \\
0 & 0 & 0 & 0 & 1 & 0 & 0 & 0 \\
12.96989 & 10.32532 & -0.56926 & 0 & 0 & 0 & 0 & 0
\end{bmatrix}
$$

D

$$
\begin{bmatrix}
0 & 0 & 0 \\
0 & 0 & 0 \\
0 & 0 & -0.29656
\end{bmatrix}
$$

dures. The observability analysis above suggests that the stack voltage should be used for state estimation purposes.

7 Conclusion

A control-oriented fuel cell system model has been developed using physical principles and stack polarization data. The inertia dynamics of the compressor, manifold filling dynamics and time-evolving reactant mass, humidity and partial pressure, and membrane water content are captured. This model has not been fully validated but it reflects extensive work to consolidate the open-literature information currently available. Transient experimental data, once available, can be used to calibrate the model parameters such as membrane diffusion and osmotic drag coefficients to obtain a high fidelity model. Additionally, stack flooding effects needs to be integrated into the model. Examples of application of the current model on the analysis and simulation of fuel cell systems are provided—selection of optimal system excess ratio, transient effect of step inputs, and analysis of system observability.

Acknowledgment

Appendix A: Flow Calculations

In this appendix, we first explain the calculation of mass flow rate between two volumes using nozzle equations. Then we explain the calculation of mass flow rates of each species (O_2, N_2 and vapor) into and out of the cathode channel in Appendix B. The flow rates are used in the mass balance equations (9). The nozzle flow equation [32] is used to calculate the flow between two volumes. The flow rate passing through a nozzle is a function of the upstream pressure, p_u, and downstream pressure, p_d. The flow characteristic is divided into two regions according to the critical pressure ratio:

$$
pr_{crit} = \left(\frac{p_d}{p_u}\right)_{crit} = \left(\frac{2}{\gamma+1}\right)^{\gamma/(\gamma-1)} \tag{A1}
$$

where $\gamma = C_p/C_v$ is the ratio of the specific heat capacities of the gas. For sub-critical (normal) flow where pressure drop is less than the critical pressure ratio, $pr > pr_{crit}$, the mass flow rate is calculated from

$$
W = \frac{C_D A_T p_u}{\sqrt{RT_u}} (pr)^{1/\gamma} \left\{ \frac{2\gamma}{\gamma-1} \left[1 - (pr)^{(\gamma-1)/\gamma} \right] \right\}^{1/2} \tag{A2}
$$

where T_u is the upstream gas temperature, C_D is the discharge coefficient of the nozzle, A_T is the opening area of the nozzle (m^2) and R is the universal gas constant. For critical (choked) flow, $pr \leqslant pr_{crit}$, the mass flow rate is given by

$$
W_{choked} = \frac{C_D A_T p_u}{\sqrt{RT_u}} \gamma^{1/2} \left(\frac{2}{\gamma+1}\right)^{(\gamma+1)/(2(\gamma-1))} \tag{A3}
$$

If the pressure difference across the nozzle is small, the flow rate can be calculated from the linearized equation

$$
W = k_{nozzle}(p_u - p_d) \tag{A4}
$$

Appendix B: Standard Thermodynamic Calculations

Typically, air flow properties are given in terms of total mass flow rate, W, pressure, p, temperature, T, relative humidity (RH), ϕ, and dry air oxygen mole fraction, y_{O_2}. We then use thermodynamic properties to calculate the mass flow rate of the individual species. Although these equations are standard, for completeness and educational purposes we include here all the detailed calculations associated with converting $\{W, p, T, \phi, y_{O_2}\}$ to $\{W_{O_2}, W_{N_2}, W_v\}$. Given the total flow, the humidity ratio is first used to separate the total flow rate into the flow rates of vapor and dry air. Then, the dry air flow rate is divided into oxygen and nitrogen flow rates using the definition of y_{O_2}. Assuming ideal gases, the vapor pressure is calculated from the definition of the relative humidity.

$$
p_v = \phi p_{sat}(T) \tag{B1}
$$

where $p_{sat}(T)$ is the vapor saturation pressure. Since humid air is a mixture of dry air and vapor, the dry air partial pressure is the difference between total pressure and vapor pressure $p_a = p - p_v$. The humidity ratio, ω, defined as a ratio between mass of vapor and mass of dry air in the gas

$$
\omega = \frac{M_v}{M_a} \frac{p_v}{p_a} \tag{B2}
$$

where M_v and M_a are vapor molar mass and dry air molar mass, respectively. M_a is calculated from

$$
M_a = y_{O_2} M_{O_2} + (1 - y_{O_2}) M_{N_2} \tag{B3}
$$

where M_{O_2} and M_{N_2} are the molar mass of oxygen and nitrogen, respectively. The oxygen mole fraction y_{O_2} is 0.21 for the inlet air and is lower for the exit air. The flow rate of dry air and vapor are

$$
W_a = \frac{1}{1+\omega} W \tag{B4}
$$

$$
W_v = W - W_a \tag{B5}
$$

and the oxygen and nitrogen mass flow rates can be calculated from

$$W_{O_2} = x_{O_2} W_a \qquad (B6)$$

$$W_{N_2} = (1 - x_{O_2}) W_a \qquad (B7)$$

where $x_{O_2} \equiv m_{O_2}/m_{dryair}$ is the oxygen mass fraction which is a function of dry air oxygen mole fraction, y_{O_2},

$$x_{O_2} = \frac{y_{O_2} M_{O_2}}{y_{O_2} M_{O_2} + (1 - y_{O_2}) M_{N_2}} \qquad (B8)$$

The calculation of hydrogen and vapor flow rates into the anode is similar to that of the air into the cathode, and is simpler because the anode gas only contains hydrogen and vapor.

Nomenclature

A_{fc} = Fuel cell active area (cm^2)
A_T = Valve opening area (m^2)
C_D = Throttle discharge coefficient
C_p = Specific heat ($J \cdot kg^{-1} \cdot K^{-1}$)
D_w = Membrane diffusion coefficient (cm^2/sec)
E = Fuel cell open circuit voltage (V)
F = Faraday's number (Coulombs)
I = Stack current (A)
J = Rotational inertia ($kg \cdot m^2$)
M = Molecular Mass (kg/mol)
P = Power (Watt)
R = Gas constant or electrical resistance (Ω)
T = Temperature (K)
V = Volume (m^3)
W = Mass flow rate (kg/sec)
a = Water activity
c = Water concentration (mol/cm^3)
d_{cp} = Compressor diameter (m)
i = Current density (A/cm^2)
m = Mass (kg)
n = Number of cells
n_d = Electro-osmotic drag coefficient
p = Pressure (Pa)
t = Time (s)
t_m = Membrane thickness (cm)
u = System input
v = Voltage (V)
x = Mass fraction or system state vector
y = Mole fraction or system measurements
γ = Ratio of the specific heats of air
η = Efficiency
λ = Excess ratio or water content
ρ = Density (kg/cm^3)
τ = Torque (N-m)
ϕ = Relative humidity
ω = Rotational speed (rad/s)

Subscripts

act = Activation Loss
air = Air
an = Anode
ca = Cathode
$conc$ = Concentration Loss
cp = Compressor
fc = Fuel cell
gen = Generated
in = Inlet
m = Membrane
$membr$ = Across membrane
ohm = Ohmic loss
out = Outlet
rm = Return manifold

sm = Supply manifold
st = Stack
v = Vapor
w = Water

References

[1] Yang, W.-C., Bates, B., Fletcher, N., and Pow, R., *Control Challenges and Methodologies in Fuel Cell Vehicle Development*, SAE Paper 98C054.
[2] Guzzella, L., 1999, *Control Oriented Modelling of Fuel-Cell Based Vehicles*, Presentation in NSF Workshop on the Integration of Modeling and Control for Automotive Systems.
[3] Amphlett, J. C., Baumert, R. M., Mann, R. F., Peppley, B. A., and Roberge, P. R., 1995, *Performance modeling of the Ballard Mark IV solid polymer electrolyte fuel cell*, J. Electrochem. Soc., **142**(1), pp. 9–15.
[4] Bernardi, D. M., and Verbrugge, M. W., 1992, *A Mathematical model of the solid polymer electrolyte fuel cell*, J. Electrochem. Soc., **139**(9), pp. 2477–2491.
[5] Lee, J. H., and Lalk, T. R., 1998, *Modeling fuel cell stack systems*, J. Power Sources, **73**, pp. 229–241.
[6] Springer, T. E., Zawodzinski, T. A., and Gottesfeld, S., 1991, *Polymer Electrolyte Fuel Cell Model*, J. Electrochem. Soc., **138**(8), pp. 2334–2342.
[7] Barbir, F., Balasubramanian, B., and Neutzler, J., 1999, *Trade-off design analysis of operating pressure and temperature in PEM fuel cell systems*, Proceedings of the ASME Advanced Energy Systems Division, v. 39, pp. 305–315.
[8] Friedman, D. J., Egghert, A., Badrinarayanan, P., and Cunningham, J., *Balancing stack, air supply and water/thermal management demands for an indirect methanol PEM fuel cell system*, SAE Paper 2001-01-0535.
[9] Akella, S., Sivashankar, N., and Gopalswamy, S., 2001, *Model-based systems analysis of a hybrid fuel cell vehicle configuration*, Proceedings of 2001 American Control Conference.
[10] Atwood, P., Gurski, S., Nelson, D. J., Wipke, K. B., and Markel, T., 2001, *Degree of hybridization ADVISOR modeling of a fuel cell hybrid electric sport utility vehicle*, Proceedings of 2001 Joint ADVISOR/PSAT vehicle systems modeling user conference, pp. 147–155.
[11] Boettner, D. D., Paganelli, G., Guezennec, Y. G., Rizzoni, G., and Moran, M. J., 2001, *Component power sizing and limits of operation for proton exchange membrane (PEM) fuel cell/battery hybrid automotive applications*, Proceedings of 2001 ASME International Mechanical Engineering Congress and Exposition.
[12] Turner, W., Parten, M., Vines, D., Jones, J., and Maxwell, T., 1999, *Modeling a PEM fuel cell for use in a hybrid electric vehicle*, Proceedings of the 1999 IEEE 49th Vehicular Technology Conference, v.2, pp. 1385–1388.
[13] Boettner, D. D., Paganelli, G., Guezennec, Y. G., Rizzoni, G., and Moran, M. J., 2001, *Proton exchange membrane (PEM) fuel cell system model for automotive vehicle simulation and control*, Proceedings of 2001 ASME International Mechanical Engineering Congress and Exposition.
[14] Hauer, K.-H., Friedmann, D. J, Moore, R. M., Ramaswamy, S., Eggert, A., and Badrinarayana, P., *Dynamic Response of an Indirect-Methanol Fuel Cell Vehicle*, SAE Paper 2000-01-0370.
[15] Padulles, J., Ault, G. W., Smith, C. A., and McDonald, J. R., 1999, *Fuel cell plant dynamic modeling for power systems simulation*, Proceedings of 34th Universities Power Engineering Conference, v. (**34**),1, pp. 21–25.
[16] Pischinger, S., Schönfelder, C., Bornscheuer, W., Kindl, H., and Wiartalla, A., *Integrated Air Supply and Humidification Concepts for Fuel Cell Systems*, SAE Paper 2001-01-0233.
[17] Watanabe, M., Uchida, H., Emori, M., April 1998, *Analyses of Self-Humidification and Suppression of Gas Crossover in Pt-Dispersed Polymer Electrolyte Membranes for Fuel Cells*, J. Electrochem. Soc., **145**(4), pp. 1137–1141.
[18] Larminie, J. and Dicks, A., 2000, *Fuel Cell Systems Explained*, West Sussex, England, John Wiley & Sons Inc.
[19] Lee, J. H., Lalk, T. R., and Appleby, A. J., 1998, *Modeling electrochemical performance in large scale proton exchange membrane fuel cell stacks*, J. Power Sources, **70**, pp. 258–268.
[20] Kordesch, K. and Simader, G., 1996, *Fuel Cells and Their Applications*, Weinheim, Germany, VCH.
[21] Laurencelle, F., Chahine, R., Hamelin, J., Agbossou, K., Fournier, M., Bose, T. K., and Laperriere, A., 2001, *Characterization of a Ballard MK5-E proton exchange membrane fuel cell stack*, Fuel Cells Journal, **1**(1), pp. 66–71.
[22] Amphlett, J. C., Baumert, R. M., Mann, R. F., Peppley, B. A., Roberge, P. R., and Rodrigues, A., 1994, *Parametric modelling of the performance of a 5-kW protonexchange membrane fuel cell stack*, J. Power Sources, **49**, pp. 349–356.
[23] Nguyen, T. V., and White, R. E., 1993, *A Water and Heat Management Model for Proton-Exchange-Membrane Fuel Cells*, J. Electrochem. Soc., **140**(8), pp. 2178–2186.
[24] Mann, R. F. et al., 2000, *Development and application of a generalized steady-state electrochemical model for a PEM fuel cell*, J. Power Sources, **86**, pp. 173–180.
[25] Baschuk, J. J., and Li, X., 2000, *Modeling of polymer electrolyte membrane fuel cells with variable degrees of water flooding*, J. Power Sources, **86**, pp. 186–191.
[26] Dutta, S., Shimpalee, S., and Van Zee, J. W., 2001, *Numerical prediction of mass-exchange between cathode and anode channels in a PEM fuel cell*, Int. J. Heat Mass Transfer, **44**, pp. 2029–2042.

[27] Moraal, P. and Kolmanovsky, I., *Turbocharger Modeling for Automotive Control Applications*, SAE Paper 1999-01-0908.

[28] Cunningham, J. M., Hoffman, M. A., Moore, R. M., and Friedman, D. J., *Requirements for a Flexible and Realistic Air Supply Model for Incorporation into a Fuel Cell Vehicle (FCV) System Simulation*, SAE Paper 1999-01-2912.

[29] Adams, J. A., Yang, W-C., Oglesby, K. A., and Osborne, K. D., *The development of Ford's P2000 fuel cell vehicle*, SAE Paper 2000-01-1061.

[30] Gravdahl, J. T. and Egeland, O., 1999, *Compressor Surge and Rotating Stall*, Springer, London.

[31] Kailath, T., 1980, *Linear Systems*, Prentice-Hall, New Jersey.

[32] Thomas, P., 1999, *Simulation of Industrial Processes for Control Engineer*, London, Butterworth Heinemann.